Cellular and Molecular Life Sciences (2025) 82:109
https://doi.org/10.1007/s00018-025-05627-7

ORIGINAL ARTICLE

Endometrium-derived organoids from cystic fibrosis patients and mice as new models to study disease-associated endometrial pathobiology

Ellen De Pauw[1] · Beau Gommers[1] · Marjolein M. Ensinck[2] · Stefan Timmerman[3] · Silke De Vriendt[1] · Celine Bueds[1] · Mengjie Wei[1] · Florian Hermans[4] · Kaline Arnauts[5] · Anabela S. Ramalho[6] · Francois Vermeulen[6,7] · Lieven Dupont[2,8] · Diether Lambrechts[9,10] · Marianne S. Carlon[2] · Hugo Vankelecom[1]

Received: 15 September 2024 / Revised: 17 January 2025 / Accepted: 16 February 2025

Abstract

Cystic fibrosis (CF) is a life-shortening genetic disorder, caused by mutations in the CF transmembrane conductance regulator (CFTR) protein that regulates ion and fluid transport in epithelial tissue. Female CF patients face considerable fertility challenges, with higher prevalence of deficient fertility compared to healthy women. Not much is known about the underlying causes. In particular, the pathobiology of the endometrium, the uterus' inner lining essential for pregnancy and expressing fluctuating *CFTR* levels during the menstrual cycle, is unexplored in CF. To address this gap, we developed organoid models from CF patient endometrium. The organoids recapitulated CF characteristics and revealed molecular and pathway differences in cycle-recapitulating hormone responses compared to healthy endometrial organoids. Furthermore, specific functional aberrations were restored by CFTR modulator treatment. To further complement human organoid models for unraveling endometrial pathobiology in CF, we also developed organoids from a genetic CF mouse model that were also found to recapitulate CF characteristics. Moreover, single-cell RNA-sequencing analysis of the CF mouse uterus revealed molecular traits in the endometrium similar to the human CF endometrium (as evidenced by its organoid model). Our study provides new endometrium models to advance our understanding of CF-associated endometrial pathobiology, particularly regarding menstrual cycle aberrations that impact fertility. This research is timely since improved CF therapeutics result in increased life expectancy, allowing more CF patients to consider starting a family.

Keywords 3D models · Hormones · Fertility deficiency · CFTR modulators · Transcriptomics

✉ Hugo Vankelecom
hugo.vankelecom@kuleuven.be

[1] Laboratory of Tissue Plasticity in Health and Disease, Cluster of Stem Cell and Developmental Biology, Department of Development and Regeneration, KU Leuven (University of Leuven), Leuven, Belgium

[2] Laboratory of Respiratory Diseases and Thoracic Surgery (BREATHE), Department of Chronic Diseases and Metabolism, KU Leuven, Leuven, Belgium

[3] Department of Obstetrics and Gynecology, University Hospitals Leuven (UZ Leuven), Leuven, Belgium

[4] Department of Cardiology and Organ Systems, Biomedical Research Institute (BIOMED), Faculty of Medicine and Life Sciences, Hasselt University, Diepenbeek, Belgium

[5] Department of Chronic Diseases and Metabolism (CHROMETA), Translational Research Center for Gastrointestinal Disorders (TARGID), KU Leuven, Leuven, Belgium

[6] CF Centre, Woman and Child Unit, Department of Development and Regeneration, KU Leuven, Leuven, Belgium

[7] Department of Pediatrics, Pediatric Pulmonology, UZ Leuven, Leuven, Belgium

[8] Department of Respiratory Diseases, UZ Leuven, Leuven, Belgium

[9] VIB– Center for Cancer Biology, Leuven, Belgium

[10] Laboratory for Translational Genetics, Department of Human Genetics, KU Leuven, Leuven, Belgium

Published online: 13 March 2025

Introduction

Cystic fibrosis (CF) is the most prevalent life-shortening genetic disease in Caucasians, caused by mutations in the CF transmembrane conductance regulator (*CFTR*) gene which encodes an ion (chloride (Cl^-) and bicarbonate (HCO_3^-)) channel regulating transport of electrolytes and fluid in epithelial cells. Female CF patients (further referred to as "women with CF" (wwCF)) show decreased fertility with only half becoming pregnant without assisted reproductive technologies [1]. The estimated prevalence of sub- and infertility is higher than in the age-matched general female population (35% and 5–15%, respectively) [2]. So far, deficient fertility in wwCF has received poor attention, and not much is known on the underlying causes. Proposed reproductive-tract factors include the presence of dehydrated, viscous mucus in the cervix that may hinder sperm passage, and altered HCO_3^- balance in the uterus which may negatively impact sperm capacitation [1, 3]. However, the uterus' inner tissue or endometrium, which is essential for successful pregnancy, has only poorly been explored as plausible contributor to CF pathobiology. CFTR is expressed in the healthy endometrial epithelium, at levels fluctuating with the menstrual cycle. Its expression is regulated by the cycle-controlling ovarian hormones estrogen (E2; CFTR upregulation) and progesterone (P4; CFTR downregulation), in a pattern that correlates with the physiological cyclic changes in uterine fluid volume and composition [4–6]. Uterine luminal fluid secretion and absorption appear principally regulated by an interplay between CFTR (mediating anion and H_2O secretion) and the epithelial sodium channel ENaC (mediating sodium (Na^+) and H_2O absorption), expressed in a mirrored fashion in the cycling endometrium [7]. Apart from this very confined knowledge on the role of CFTR in endometrial physiology, nothing is known on the pathophysiology of the endometrium in wwCF. One main reason is the lack of reliable and tractable study models, considering the major technical and ethical hurdles to study events that occur hidden in the womb. Previously, our group developed organoid models from mouse and human endometrium as novel and powerful tools to study the tissue's (patho-) physiology [8, 9]. Healthy endometrium-derived organoids were found to reliably capture the original tissue's characteristics as well as reproduce epithelium biology including recapitulation of key characteristics of the proliferative and secretory phase of the menstrual cycle following defined exposure to E2 and P4 [8, 10]. Organoids from endometrial diseases such as endometriosis and cancer were shown to recapitulate the specific pathology's (and patient's) characteristics, indicating that diseased, deficient endometrium can also reliably be captured by organoid models [9].

To decipher endometrial pathobiology in CF, we here developed organoids from CF patient and CF mouse endometrium, both of which were found to recapitulate CF characteristics. CFTR modulators were shown to rescue CF endometrial organoids' aberrant behavior. CF patient-derived organoids and single-cell transcriptomic analysis of the CF mouse uterus revealed molecular, pathway and cellular differences compared to the healthy counterparts. Our study and models allow to explore CF endometrial pathobiology at the molecular and functional level and identify its contribution to decreased fertility in wwCF. This endeavor is of particular interest since improved CF treatments, especially the highly effective CFTR modulator therapies (HEMT), have substantially increased life expectancy and quality of life of CF patients which allows them to more often consider starting a family.

Materials & methods

The workflow and experimental design of the study is presented in Fig. S1A.

Development and hormone exposure of organoids from CF patient endometrium

Endometrial biopsies were obtained at University Hospitals (UZ) Leuven, after informed written consent, from wwCF and from controls (i.e. healthy volunteers or patients undergoing laparoscopy for benign non-endometrial gynecological conditions). The control women all tested negative for *CFTR* carrier status of *F508del*. The study was approved by the Ethical Research Committee UZ/KU Leuven (S66294, S59006, S65570) and is compliant with all relevant ethical regulations regarding research involving human participants.

The tissue samples were mechanically and enzymatically dissociated into small fragments and single cells, which were resuspended in 70% Matrigel (Corning)/30% DMEM/F12 (Thermo Fisher Scientific) supplemented with Rock inhibitor (RI, Y-27632, Merck Millipore), seeded in droplets and cultured, all as previously described [8]. Organoids were passaged every 7–14 days, including dissociation with TrypLE Express (Thermo Fisher Scientific) containing RI and mechanical trituration, resuspension in 70% Matrigel/30% DMEM/F12 (supplemented with RI) and seeding, all as described before [8]. Established organoid lines were amplified, cryopreserved for biobanking and subjected to downstream analyses. Unless otherwise stated, organoids of passage number P2−P6 were used for the experiments described.

Hormone exposure to mimic the menstrual cycle phases was performed as follows [10]: after 2 days of growth in

endometrial organoid medium (EOM, Table S1A), the organoids (P2-P4) were exposed for 6 days to 10 nM β-estradiol (E2, Sigma), or for 2 days to 10 nM E2 followed by 4 days to a combination of 10 nM E2, 1 µM P4 (Sigma), 0.25 mM cyclic adenosine monophosphate (cAMP, Tocris) and 10 µM Wnt inhibitor XAV-939 (Tocris) (referred to as "EPCX"). Medium was refreshed every 2 days. Organoids were collected at the end of hormone exposure (day 8) for further analysis. In specific experiments, E2 exposure was combined with elexacaftor/tezacaftor/ivacator treatment (ETI, Selleckchem; all at 3 µM) or vehicle (dimethylsulfoxide (DMSO)). ETI or vehicle was added every 2 days. Brightfield pictures of organoid cultures were recorded using an Axiovert 40 CFL microscope (Zeiss). Brightfield time-lapse pictures were recorded with the Incucyte S3 (Sartorius). Organoid diameter was measured with Fiji imaging software (https://imagej.net/ij/).

To monitor apoptosis in organoids exposed to E2 (see above for schedule), Incucyte Caspase-3/7 dye (Sartorius; 5 µM) was added on day 7 for 24 h followed by fluorescent signal recording. As a positive control for detection of apoptosis, organoids (CFEO) were exposed to staurosporine (Tocris; 24 h from day 7 to 8 at 1 µM; added together with the Incucyte Caspase-3/7 dye). Brightfield and fluorescence pictures of organoid cultures were recorded using the THUNDER Imager (Leica Microsystems).

Development and hormone exposure of organoids from CF mouse endometrium

Cftr^{tm1Eur} mice, harboring a *F508del* mutant exon in the *Cftr* gene (which does not interfere with its transcription), were used [11]. Animals were housed in conditions of constant temperature, humidity and day-night cycle, and *ad libitum* access to water and food. All animal experiments were approved by the KU Leuven Ethical Committee for Animal Experimentation (P072/2024). Genotype was determined with ear biopsy-derived genomic DNA using Sanger sequencing. PCR products were purified using ExoSAP-IT Express reagent (Thermo Fisher Scientific), combined with sequencing primers (Table S1B) and sequenced by Eurofins Genomics. Chromas software (Technelysium) was used to identify wild-type (WT; F508$^{wt/wt}$) and CF (F508$^{del/del}$) genotype. Laxative (Movicol) was added to the drinking water to avoid intestinal obstruction in CF mice. To quantitatively assess the fertility of female mice, 13–14 weeks old WT or CF females were continuously mated to WT males for 5 months and monitored daily for litters born and number of pups. For organoid development, adult WT and CF mice of 13–15 weeks old were used. Organoids were established from mouse endometrium as in detail described before [8]. In brief, the tissue was dissociated, seeded in 70% Matrigel/DMEM/F12 droplets and cultured in defined medium (Table S1C) to induce mouse endometrial organoid (mEO) formation and growth. Slight modifications were applied including enzymatic incubation with collagenase IV (1 mg/mL in DMEM/F12) instead of EDTA solution, and medium composition optimizations (as reported in [12]). Every 7–14 days, organoids were passaged as described [8]. To mimic the estrus cycle phase, organoids were grown for 4 days in mEO medium followed by treatment with 1 nM E2 (Sigma) for 2 days [8].

Development and culture of rectal CF organoids

To highlight the difference in morphology in CF endometrial *versus* rectal organoids (which may point to alternative ion channel contribution to organoid swelling), CF rectal organoids were established from rectal biopsies (as described before [13]) originating from a selection of CF patients of which CFEO had been generated. In short, intestinal crypts were isolated from the tissue samples and plated in Matrigel. Organoids were grown for 7 days, mechanically dissociated and re-seeded. Brightfield pictures of organoid cultures were recorded using the Axiovert 40 CFL microscope. Collection of rectal biopsies was approved by the Ethical Research Committee UZ/KU Leuven (S56329).

Forskolin-induced swelling assay

To assess CFTR (dys)functional activity and rescue by CFTR modulators in (mouse and human) endometrial organoids, the forskolin-induced swelling (FIS) assay was performed as described previously [14]. The cAMP activator forskolin (FSK) stimulates CFTR activity leading to ion and H_2O influx which causes organoid swelling. In short, organoids were exposed to FSK (Sigma Aldrich; 5 µM) and immediately monitored by confocal live cell microscopy at 37 °C for 120 min (LSM800, Zeiss; Zen Blue software). The increase in total organoid size (area) normalized to the organoid size (area) at timepoint (t) 0 of FSK addition was quantified with Fiji imaging software. In specific experiments, organoids were treated with CFTR modulators elexacaftor/tezacaftor (ET; both at 3 µM, 24 h pre-incubation) or ET pre-incubation with ivacaftor (ETI; all at 3 µM, ivacaftor added together with FSK), or with a specific CFTR inhibitor Inh172 (Selleckchem; 50 µM, 4 h pre-incubation, followed by 50 µM during the FIS assay), or with vehicle (DMSO).

Halide-sensitive YFP assay

To evaluate CFTR (dys)functional activity and rescue by CFTR modulators in human endometrial organoid-derived monolayers, the halide-sensitive (HS)-YFP assay was

applied which measures CFTR activity by degree of HS-YFP quenching due to CFTR-dependent iodide (I^-) influx. Organoids were dissociated into single cells, transduced with HS-YFP-encoded lentiviral vector [15], and regrown after seeding in Matrigel droplets as described above. After 10–14 days, the HS-YFP-transduced organoids were dissociated into single cells which were plated onto a 3% Matrigel layer to grow into confluent monolayers within 7–8 days. In specific experiments, monolayers were incubated with ET (3 µM, 24 h pre-incubation), Inh172 (20 µM, 24 h pre-incubation, followed by 50 µM during assay) or vehicle (DMSO). Ivacaftor (3 µM) and/or FSK (10 µM) was added for 20 min. Fluorescence (F0) was measured using Perkin Elmer Envision for 5 s after which I^- buffer (137 mM NaI, 2.7 mM KI, 1.7 mMKH2PO4, 10.1 mM Na2HPO4, 5 mM D-glucose) was injected into the well and fluorescence monitored for another 20 s (F). HS-YFP quenching was determined at the end of the interval as F/F0, and CFTR function as 1−(F/F0) [15]. Brightfield and fluorescence pictures of organoid cultures were recorded using the Axiovert 40 CFL microscope.

Bulk RNA-sequencing analysis

Human endometrial organoids were collected at the end of hormone exposure (see above). CF endometrium-derived organoids (CFEO; from $n=4$ patients) and healthy endometrium-derived organoids (HEO; $n=4$) were subjected to bulk RNA-sequencing (RNA-seq) to assess overall transcriptomic differences. RNA was extracted using the RNeasy Micro kit (Qiagen). RNA concentration and purity were determined using the Nanodrop ND-8000 (Nanodrop Technologies) and RNA integrity and concentration were assessed using the BioAnalyzer RNA Nano kit (Agilent). Libraries were constructed with the Illumina Stranded mRNA Sample Prep Kit, followed by sequencing on Illumina NovaSeq 6000 (Illumina) at the VIB Nucleomics Core (https://nucleomicscore.sites.vib.be/en). Data are accessible from ArrayExpress database (accession number E-MTAB-14456). Quality control of raw reads was performed with FastQC v0.11.7 [16]. Adapters were filtered using Trimmomatic v0.39 [17]. Splice-aware alignment was carried out using Hisat2 [18] against the reference genome (hg38) and with the transcriptome version (Release-109) employing default parameters. Quantification of reads per gene was conducted using FeatureCounts from the Subread package [19]. Count-based differential expression analysis was performed using the R-based Bioconductor package DESeq2 [20]. Volcano plots were generated using the EnhancedVolcano package (v1.20.0). Gene Ontology (GO) enrichment analysis of differentially expressed genes (DEGs; fold change (FC)>1.5 and p-value<0.05) was executed with the ClusterProfiler R package (v4.10.1), generating EnrichGO, Reactome and WikiPathways outputs. Heatmaps were generated using the pheatmap package (v1.0.12). Normalized gene expression counts were used as input, with Z-scores calculated across each gene (row-wise scaling). Of note, p-adjusted values (p-adjust, after Benjamini-Hochberg testing) could not be applied for DEG/volcano plot and succeeding GO enrichment analyses because of the yet limited number of samples (with inter-patient variability). Therefore, a cut-off based on uncorrected p-values (<0.05) was used. Significantly enriched GO terms or pathways (p-adjust<0.05) were determined from these analyses. Of note, because of an insufficient number of organoids of HEO-4 at time of hormone exposure, the E2 condition for HEO-4 was not available for sequencing. Hence, analyses (heatmaps) comparing matched EOM/E2/EPCX-treated HEO only include 3 samples.

Single-cell RNA-sequencing analysis

Uteri from 14–15 weeks old WT and CF mice, evaluated for estrous cycle phase by vaginal smear cytology, were dispersed into single cells using collagenase IV (1 mg/mL in DMEM/F12), filtered through a 40 µm filter and subjected to single-cell RNA-sequencing (scRNA-seq) analysis using 10X Genomics technology to assess transcriptome differences at the single-cell level. Cells were loaded onto a cartridge and single-cell capture, barcoding and library preparation performed using 10x Chromium next GEM single cell 3' v3.1. chemistry according to the manufacturer's protocol (10x Genomics). Libraries were sequenced using a NovaSeq 6000 (Illumina). After quality control, raw sequencing reads were demultiplexed, aligned to the mouse reference genome (mm10-2020-A) and gene expression matrices were generated, all according to the CellRanger pipeline (v5.0.0; 10x Genomics). Downstream bioinformatic analysis was performed in R (v.4.3.3) using Seurat (v.5.1.0) [21]. Dead and low-quality cells and potential doublets (i.e. with <750 genes or >5,000 genes and >10% mitochondrial RNA) were removed.

The single-cell transcriptomes of all WT and CF uteri were integrated following the Seurat (v5.1.0) integration workflow. Filtered matrices were combined, normalized (using NormalizeData function), and variable features were identified (using FindVariableFeatures function), followed by scaling of expression levels (using ScaleData function) and principal component analysis (using RunPCA). Integration, based on anchor-based Reciprocal Principal Component Analysis (RPCA), was performed using IntegrateLayers function. The top 34 principal components were selected and used for Uniform Manifold Approximation and Projection (UMAP) dimensionality reduction [22],

creating an eventual UMAP of 17 clusters (with 0.5 clustering resolution using FindClusters function). Clusters were annotated based on canonical markers, including recent scRNA-seq studies of mouse uteri [23–25]. DEG analysis was performed using the FindMarkers function with parameters min. pct = 0.25, logfc.threshold = 0.50 and using MAST as test method (MAST package; v1.28.0) [26]. GO analysis of biological processes was done on the significant DEGs (false discovery rate (FDR) < 0.05 and avg_log2FC > 0.50) using Panther (generating Panther and Reactome pathways outputs; v.19.0) [27]. Raw sequencing data are available at ArrayExpress (accession number E-MTAB-14455).

Gene expression analysis by RT-qPCR

Total RNA from mouse and human tissue samples and organoids (the latter collected from two 20 µL Matrigel droplets, containing about 300 organoids/droplet) was isolated using the RNeasy Micro kit (Qiagen) and subjected to reverse transcription (RT) with Superscript III First-Strand Synthesis Supermix (Invitrogen). Following RT, real-time quantitative PCR (qPCR) was performed using the Platinum SYBR Green qPCR SuperMix-UDG (Invitrogen) and specific forward and reverse primers (Table S1B, D), as described before [8]. β-actin (*Actb*) and glyceraldehyde-3-phosphate dehydrogenase (*GAPDH*) were used as housekeeping genes for normalization of mouse and human data, respectively. Normalized gene expression levels are shown as bar graphs of delta (d)Ct values (Ct target − Ct housekeeping gene). The number of biological replicates (tissue or organoids derived from different, individual patients or mice) are indicated by the data points in the graphs and also stated in the legends of the figure.

Histochemical and immunostaining analysis

Mouse and human tissue and organoid samples were fixed in 4% paraformaldehyde (Merck), embedded in paraffin and sections subjected to hematoxylin and eosin (H&E) staining (H&E staining kit, Abcam) or immunofluorescence staining as described before [28]. In short, antigen retrieval (10 mM citrate, pH6) and permeabilization (0.1% Triton X-100, Sigma-Aldrich) were performed, followed by blocking with bovine serum albumin, glycine and donkey serum (Merck). Slides were incubated overnight with primary antibodies targeting E-cadherin (ECAD, Cat. No. 3195, Cell Signaling Technology), Ki67 (Cat. No. 556003, BD Biosciences), cytokeratin 8 and 18 (CK8/18, Cat. No. GP11, Progen), forkhead box protein A2 (FOXA2, Cat. No. AB108422, Abcam) and CC3 (Cat. No. AB3623, EMD Millipore) (Table S1E). Following incubation with secondary antibodies (Table S1F) and nuclear counterstaining with Hoechst33342 (Merck), sections were mounted with ProLong Gold (Thermo Fisher Scientific) or DPX mountant (Sigma-Aldrich). Images were recorded using a Leica DM5500 upright epifluorescence microscope (Leica 576 Microsystems), and converted to pictures for figures with Fiji imaging software.

As positive control for CC3 immunostaining, organoids (CFEO) were exposed for 24 h to staurosporine (1 µM), and subjected to the immunofluorescence staining protocol as described above (Fig. S3B). As negative control, primary antibody was omitted during the staining procedure in which case no signal was observed (Fig. S3B). Other antibodies were validated before [8] and relevant publications are listed on the company's website page of the product, together with certificates of analysis.

Statistical analysis

Statistical analysis was performed using Graphpad Prism (v10.3.1; GraphPad Software). (Un)paired two-tailed Student's t-test was applied for comparison of 2 groups. When comparing more groups, one-way analysis of variance (ANOVA) was used when considering one variable, followed by the correct multiple comparisons tests. Statistical significance was defined as $p < 0.05$.

Results

Endometrium-derived organoids recapitulate the CFTR expression pattern of the in vivo cycling endometrium

To validate the endometrium-derived organoid model as a valuable and reliable tool to study CFTR (dys)function in endometrial (patho)biology, we examined whether expression of *CFTR*, as well as *ENAC* (i.e. its *SCNN1A*, *SCNN1B* and *SCNN1G* subunits), in endometrial organoids recapitulate the in vivo cyclic expression pattern. Following defined exposure to the ovarian hormones E2 and P4 to replicate the menstrual cycle phases (Fig. 1A) [8, 10], *CFTR* expression showed a significant decline in HEO from proliferative (+E2) to (mid-)secretory (+EPCX) phase, as analyzed by bulk RNA-seq (Fig. 1B) and validated by RT-qPCR (Fig. 1C). Of note, highest *CFTR* expression was observed in the organoid stem-cell condition (i.e. in the stem cell-maintaining and -promoting EOM) [8, 9] (Fig. 1B, C; Table S1A), suggesting that *CFTR* is most highly expressed in the endometrial stem cell state. *LGR5*, previously proposed as endometrial stem cell marker [29, 30], showed similar expression dynamics in HEO from stem-cell condition (EOM) to proliferative (+E2) and secretory (+EPCX) phase (Fig. 1B, C). Moreover, *CFTR* expression is predominantly

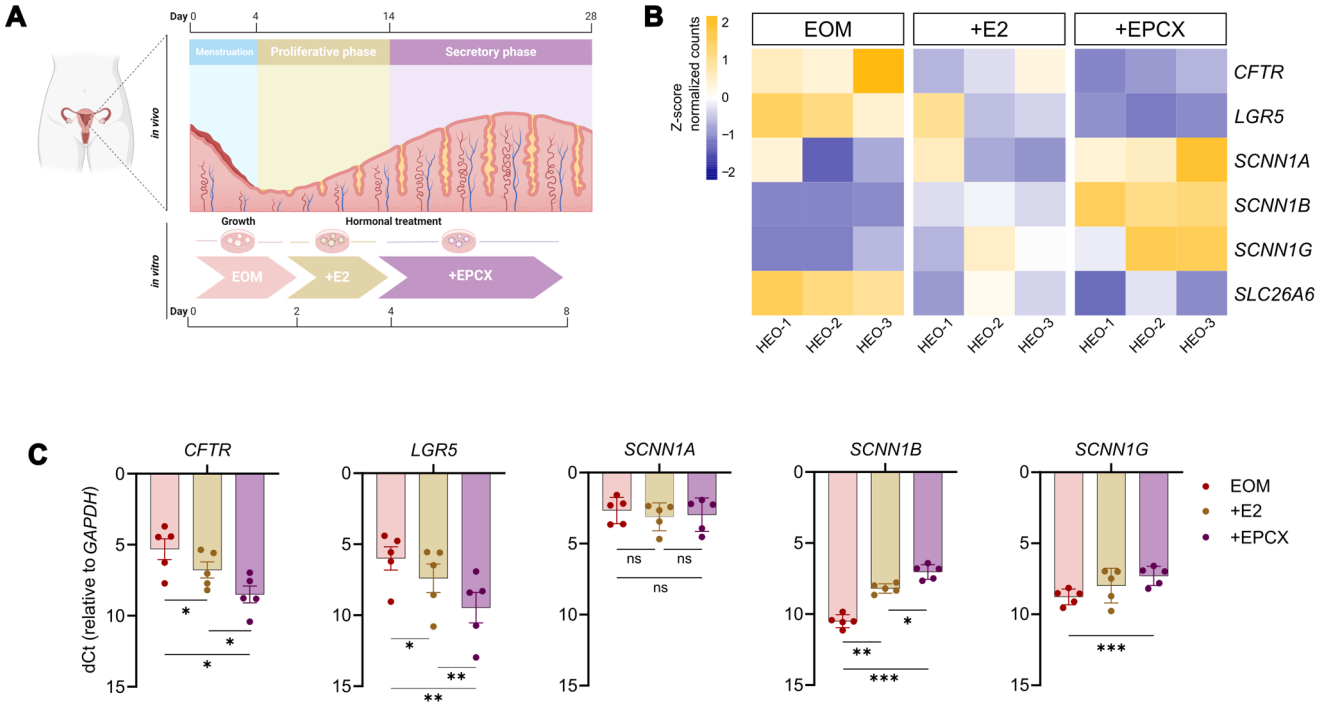

Fig. 1 Hormonal regulation of CFTR and ENAC expression in healthy endometrial organoids. **A** Schematic representation of in vitro hormone exposure of endometrial organoids to recapitulate the in vivo proliferative and (mid-)secretory menstrual cycle phases. EOM, endometrial organoid medium; E2, estradiol; EPCX, E2 + progesterone (P4) + cAMP + XAV. Created with BioRender.com. **B** Heatmap displaying scaled expression (represented as z-score of normalized counts, see color scale) of indicated genes in HEO in EOM and following E2 and EPCX exposure, as determined by bulk RNA-seq analysis. **C** Relative gene expression levels of indicated genes in HEO in EOM and following E2 and EPCX exposure, as determined by RT-qPCR. Bar graphs show mean ± SEM ($n = 5$ biological replicates, indicated by data points); oneway ANOVA with Tukey's multiple comparison test; $*p < 0.05$, $**p < 0.01$, $***p < 0.001$

observed in the cell subcluster in which *LGR5* expression is most prominent, as assessed using a published scRNA-seq dataset from human healthy ex vivo endometrium [31] (Fig. S1B). Notably, *CFTR* expression in the intestine is similarly found in the stem cells and decreases from the crypt stem cell compartment toward the differentiated villus cells [32]. Also, *CFTR* expression is high in intestinal stem cell organoid-derived models and downregulated upon differentiation [32]. Interestingly, *ENAC* showed the opposite expression pattern in HEO, thereby recapitulating known in vivo aspects [4–6], with mainly the β-subunit (*SCNN1B*) significantly increasing upon the sequential hormone-driven differentiation to proliferative (+E2) and secretory (+EPCX) phase (Fig. 1B, C). Intriguingly, expression of this *SCNN1B* shows the strongest convergence with *CFTR* expression in the scRNA-seq-based endometrial cell clustering (Fig. S1B). Finally, expression of other ion channels known to fluctuate in parallel with *Cftr* such as *Slc26a6* (as observed in rodent uterus during the estrous cycle [33, 34]) also showed *CFTR*-comparable expression dynamics in the human organoids upon hormonal treatment (Fig. 1B).

Taken together, these findings indicate that the endometrial organoid model provides a valuable tool to study CFTR (and ENAC and other ion channels) in endometrial (patho) biology.

Organoids can be developed from CF patient endometrium and recapitulate CFTR dysfunction

In this first study on endometrial organoids from wwCF, we focused on the *F508del CFTR* mutation, as it is the most prevalent, found in 85% of the patients [35]. Endometrial biopsies (from $n = 9$ *F508del/F508del* wwCF, aged 23–40 yrs) were subjected to the organoid protocol previously defined for HEO [8]. Organoids successfully developed from CF endometrium within 7–12 days at 100% efficiency, in a way comparable to HEO (Fig. 2A and Fig. S2A). The CFEO were amenable to long-term expansion (Fig. S2B), comparable to HEO as well (Fig. S2B and [8]). Organoids typically recapitulate the epithelial compartment of the tissue of origin [8]. The CFEO indeed display an epithelial character (i.e. immunopositive for ECAD and CK8/18) and show expression of endometrium epithelial markers (such as the glandular marker FOXA2) (Fig. S2C), all as demonstrated before in HEO [8]. Remarkably, CFEO displayed a morphology not different from HEO, both showing a comparable overt lumen and similar organoid diameters

along growth in culture (Fig. 2A, B). This similar-to-healthy organoid phenotype is different from *F508del/F508del* CF rectal biopsy-derived organoids, as amply reported [36] and shown here for matched patient samples (Fig. S2D). These CF rectal organoids have almost no lumen as caused by CFTR dysfunction, which is in clear contrast with the inflated lumen in rectal organoids from healthy persons [36]. First, we assessed whether the inflated size of the CFEO (instead of an anticipated small size) could be linked to pronounced proliferation. However, the number of $Ki67^+$ cells (as quantified on day 8 of culture) did not significantly differ with HEO (Fig. S2E). Second, the inflated lumen in CFEO could be due to the presence of other ion and fluid-regulating channels and transporters that contribute to fluid influx. Of note, the *CFTR F508del/F508del* mutation does not impede transcription of the *CFTR* gene, as reported [35] and also observed here in CFEO (Fig. 2C, Fig. S2F). Apart from *CFTR* (and *ENAC*), we detected expression of several other ion/fluid-regulating channels and transporters in CFEO (and HEO) including *TMEM16A/ANO1* and *SLC26A9* (Fig. 2C, Fig. S2F), which may account for the basally inflated phenotype of the CF (as well as healthy) endometrial organoids (as also observed in CF nasal and bronchial epithelium-derived organoids [37–39]).

CFTR function in organoids is typically assessed using the FIS assay [14]. HEO showed swelling upon FSK exposure although small (Fig. 2D), likely due to their already largely inflated lumen. The swelling was found to be CFTR-dependent since this process could be counteracted by the specific CFTR inhibitor Inh172 [40] (Fig. 2D). Such FSK-induced swelling was not observed in CFEO (Fig. 2D), thereby confirming loss of CFTR function. Exposure of CFEO to the CFTR modulator combination ETI showed a trend of restoring swelling upon FSK treatment, although variable along different CFEO lines and non-significant (Fig. 2E), all in line with recent findings in CF nasal organoids [37] and likely also due to the highly pre-swollen CFEO phenotype at the start. Indeed, it is known that pre-swollen organoids limit the dynamic range of accurately quantifying CFTR function and treatment responses in the FIS assay [36]. Therefore, we turned to another experimental tool to better quantify functional CFTR deficiency and its potential rescue in endometrial organoids by CFTR modulators and applied the HS-YFP quenching assay (Fig. 2F). Using monolayer cultures derived from organoids transduced with HS-YFP-encoding lentiviral vector (Fig. S2G), we observed HS-YFP quenching in HEO-derived monolayers which was prevented by pre-incubation with Inh172, thereby validating that CFTR activity specifically underlies this HS-YFP quenching (Fig. 2F). CFEO-derived cells showed a HS-YFP tracing similar to the Inh172-exposed HEO cells, thereby confirming defective CFTR function in CFEO (Fig. 2F). Exposure of CFEO to ETI re-introduced HS-YFP quenching (to ~39% of the response in HEO; Fig. 2F), thus showing at least partial rescue of the dysfunctional CFTR in CFEO (as also seen in organoids of other CF organs) [36, 37].

Taken together, our findings confirm CFTR functional deficiency in the newly established CF endometrial organoid model, thus providing a valuable tool to study human endometrium pathobiology in CF.

CF endometrial organoids show molecular/pathway characteristics associated with CF

To delve into CF endometrial pathobiology, we first analyzed the collected bulk RNA-seq data of CFEO and HEO at basal condition (i.e. EOM, without hormonal treatment, $n=4$ biological replicates (patients) for both CFEO and HEO) to identify molecular/pathway differences. 220 and 192 DEGs were up- and downregulated, respectively, in CFEO compared to HEO (Fig. 3A; Table S2A; 1.5-fold, $p<0.05$, see Materials and Methods). GO analysis of the upregulated DEGs revealed enrichment in CFEO of biological terms related to extracellular matrix (ECM) organization and collagen formation, hypoxia and (linked) glycolysis, and insulin-like growth factor (IGF) signaling (Fig. 3B; Table S2B-D), all characteristics found in CF [41–45]. Plotting the expression of genes associated with the "ECM organization" and "collagen formation" GO terms clearly shows upregulation in CF compared to healthy condition of, among others, collagens (*COL17A1*, *COL13A1*), integrins (*ITGA5*, *ITGB2*), matrix metalloproteinase (*MMP*) *3* and *SERPINE1* (which encodes plasminogen activator inhibitor-1 (PAI-1)) (Fig. 3C). The expression pattern of genes embedded in the "hypoxia" and "glycolysis" GO terms also exposes upregulation in CF *versus* healthy condition, of, among others, *SLC2A1* (which encodes glucose transporter 1 (GLUT1)) and *HK2* (encoding the glycolytic enzyme hexokinase 2 (HK2) which catalyzes the first step of glycolysis) (Fig. 3D), both known to be upregulated by hypoxia [46, 47]. In addition, hypoxia is known to increase the expression of *SERPINE1* [48, 49], linking it to ECM (re-)modeling which we observe specifically in the CFEO (Fig. 3C).

Taken together, CFEO show molecular/pathway characteristics of known CF phenotypes and thus present valuable tools to gain deeper insights into endometrial pathobiology in CF.

CF endometrial organoids show aberrant hormone response

Next, we looked into differences in CF *versus* healthy organoid responses to hormone exposure inducing the

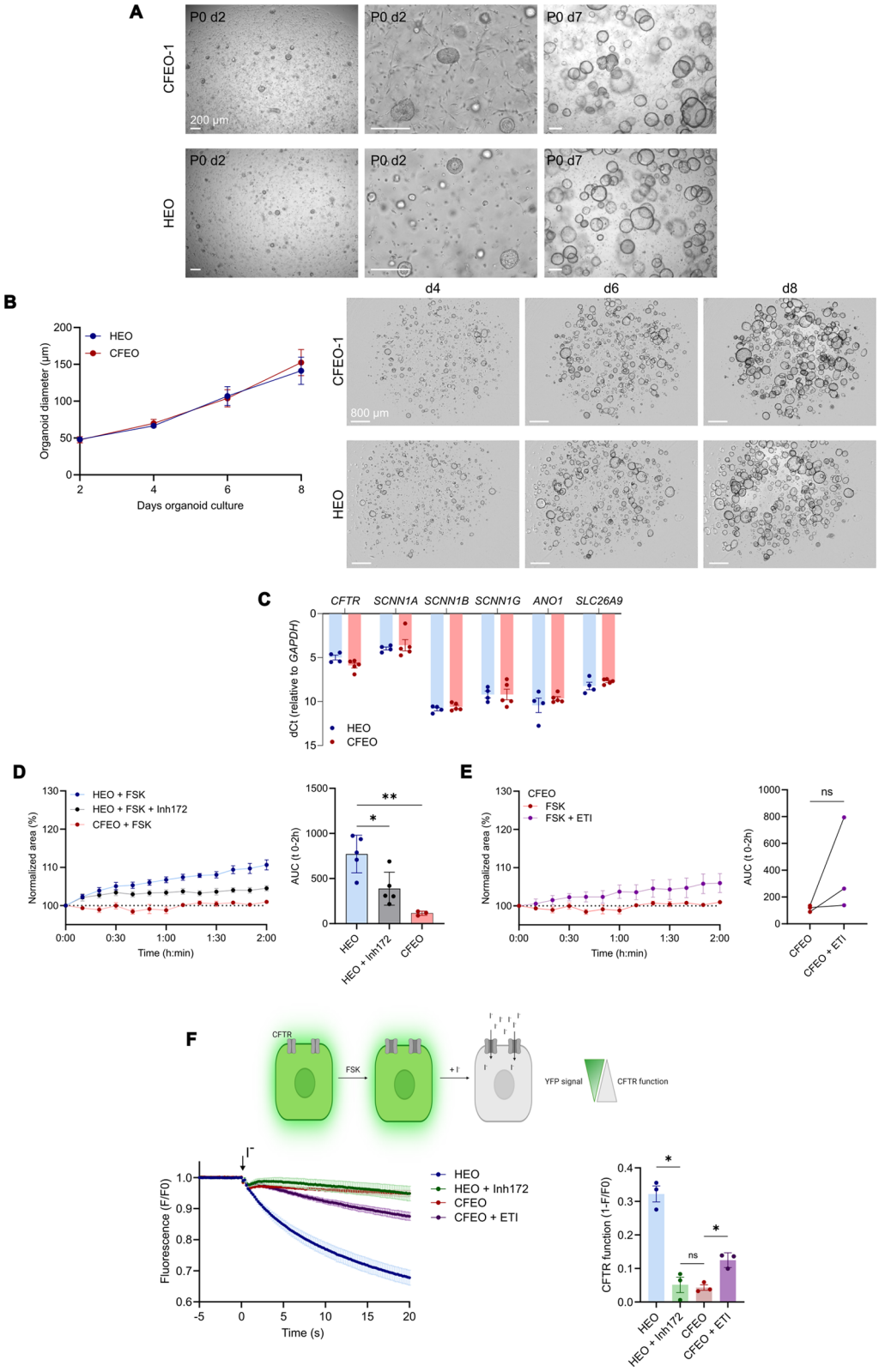
A
CFEO-1
HEO
P0 d2
P0 d7
200 µm
B
HEO
CFEO
Organoid diameter (µm)
Days organoid culture
d4
d6
d8
800 µm
C
CFTR
SCNN1A
SCNN1B
SCNN1G
ANO1
SLC26A9
dCt (relative to GAPDH)
D
HEO + FSK
HEO + FSK + Inh172
CFEO + FSK
Normalized area (%)
Time (h:min)
AUC (t 0-2h)
E
CFEO
FSK
FSK + ETI
ns
F
CFTR
FSK
YFP signal
CFTR function
Fluorescence (F/F0)
Time (s)
HEO + Inh172
CFEO + ETI
CFTR function (1-F/F0)

Fig. 2 Establishment and characterization of human CF endometrial organoids. **A** Organoid development from CF patient endometrium (CFEO) and healthy endometrium (HEO) at passage (P) 0, day (d) 2 (left and middle (magnified) panel) and d7 (right panel) of culture. **B** Time course of HEO and CFEO growth at indicated days (d) with graphs depicting median organoid diameter ($n=3$ biological replicates, ~300 organoids measured per timepoint per biological replicate) (left) and representative brightfield (BF) pictures (right), captured by Incucyte monitoring. **C** Bar graph showing relative gene expression levels of indicated genes in HEO and CFEO as determined by RT-qPCR, shown as mean ± SEM ($n=4$ and $n=5$ biological replicates for HEO and CFEO, respectively, indicated by data points). **D** FIS in HEO, treated with Inh172 or vehicle (DMSO), and in CFEO. Data are mean ± SEM ($n=5$ biological replicates for HEO, $n=3$ for CFEO, indicated by data points); two-tailed paired t-test for HEO *versus* HEO + Inh172, two-tailed unpaired t-test for HEO *versus* CFEO; $*p<0.05$, $**p<0.01$. **E** FIS in CFEO, treated with ETI or vehicle (DMSO). Data are mean ± SEM ($n=3$ biological replicates; data points are depicted in patient-matched format to show the variability in response to ETI); two-tailed paired t-test; ns, not significant. **F** Schematic representation of the HS-YFP quenching assay (top). Created with BioRender.com. Graphs depicting time course (seconds (s)) of HS-YPF quenching in HEO exposed to vehicle (DMSO) or Inh172 and CFEO exposed to vehicle (DMSO) or CFTR modulator combination ETI, after stimulation with FSK (left). Bar graph showing CFTR function measured as 1-(F/F0) (see Materials and Methods), shown as mean ± SEM ($n=3$ biological replicates, indicated by data points); two-tailed paired t-test for comparison HEO *versus* HEO + Inh172 and CFEO *versus* CFEO + ETI, two-tailed unpaired t-test for comparison HEO *versus* CFEO; $*p<0.05$, ns: not significant

proliferative (+E2) and (mid-)secretory (+EPCX) cycle phase (Fig. 1A). Strikingly, when exposed to E2, CFEO (but not HEO) cultures showed dark organoids which were found to be apoptotic (as assessed by cleaved caspase-3 (CC3) immunostaining and CC3-dye fluorescence imaging (Fig. 4A, Fig. S3A-C)). Interestingly, ETI treatment counteracted the appearance of these dark CFEO upon E2 exposure (Fig. 4B, Fig S3D).

Comparing the bulk RNA-seq data of HEO and CFEO following E2 exposure identified 338 and 331 DEGs up- and downregulated in CFEO, respectively (Fig. 4C; Table S3A). Enriched GO terms in CFEO are related to endoplasmic reticulum (ER) stress, unfolded protein response (UPR) and ER overload response (Fig. 4D; Table S3B). Plotting the expression of genes associated with these GO terms clearly demonstrates upregulation in CFEO of, among others, genes encoding ER-localized co-chaperones (*DNAJC3*, *DNAJB9*) and *WFS1*, *SSR2*, known to be involved in regulating ER stress and UPR (Fig. 4E) [50, 51].

GO terms downregulated in CFEO *versus* HEO encompass (mitotic) nuclear division, chromosome segregation and cell cycle phase transition (Fig. 4F, Table S3C), indicating cell cycle arrest in CFEO upon E2, which is further shown by the lower expression of associated cell cycle regulating and promoting genes (such as *MKI67*, *PLK*, *EDN1*; Fig. 4E).

Following EPCX exposure, 164 upregulated and 337 downregulated genes were identified (Fig. 4G; Table S4A). Since *CFTR* expression is at its lowest in this 'receptivity' phase (as induced by EPCX, Fig. 1B, C), we would expect the lowest impact of deficient CFTR in this EPCX condition. Indeed, notable upregulated GO terms could not be identified from the DEGs, but interestingly, downregulation of cilium organization/assembly/movement-related terms was found in CFEO compared to HEO upon EPCX exposure (Fig. 4H; Table S4B). Indeed, ciliated epithelial cells with motile cilia are a distinct endometrial cell population present during the receptivity phase [31]. Plotting the expression of genes associated with these GO terms shows clear downregulation in CFEO of, among others, *DNAAF1* and *DNAH11*, both encoding proteins crucial for motile cilia function and assembly [52] (Fig. S3E).

Taken together, our findings provide the first indications of aberrant responses of CF endometrium to the hormones that regulate the proliferative and secretory menstrual cycle phases, as revealed by their respective organoid models.

Enhancing the experimental toolbox to study CF endometrium pathobiology with mouse CF model

Availability of human CF endometrial material is restricted by the limited number of wwCF presenting for endometrial research and the fact that endometrial sampling of human patients comes with some challenges such as an (additional) invasive procedure that is not painless. Therefore, we implemented the $F508^{del/del}$ CF mouse model to expand the experimental toolbox for CF endometrium research [11]. $F508^{del/del}$ CF female mice display decreased fertility with reduced litter number and size (Fig. S4A), confirming previous findings with other independent CF mouse models [53], and aligning with the general notion of fertility problems in wwCF [1, 2]. Likely, several reproductive tract factors play a role, as also previously proposed [53, 54]. Here, we concentrate on potential endometrial abnormalities, as considered for patient CF above.

To generate a detailed view on cellular, molecular and pathway differences in CF *versus* healthy endometrium, we performed scRNA-seq analysis of CF and WT uteri ($n=3$ mice of each). We focused on the estrus phase (of the mouse estrous cycle) since it represents the 'fertility' (ovulation/mating) period and the phase with highest *Cftr* expression [5], thus expecting the most pronounced impact of deficient CFTR. Of note, one of the three CF mice never entered estrus during the 13 days of daily follow-up but remained in diestrus, which is in line with a previous study reporting that 30% of *Cftr* mutant mice are unable to enter estrus, thereby supporting estrous cycle irregularities as one of the contributors to decreased fertility [53]. Quality control and filtering, applied collectively on all samples (including the CF sample in diestrus phase; Fig. S4B), yielded 33,270 good-quality

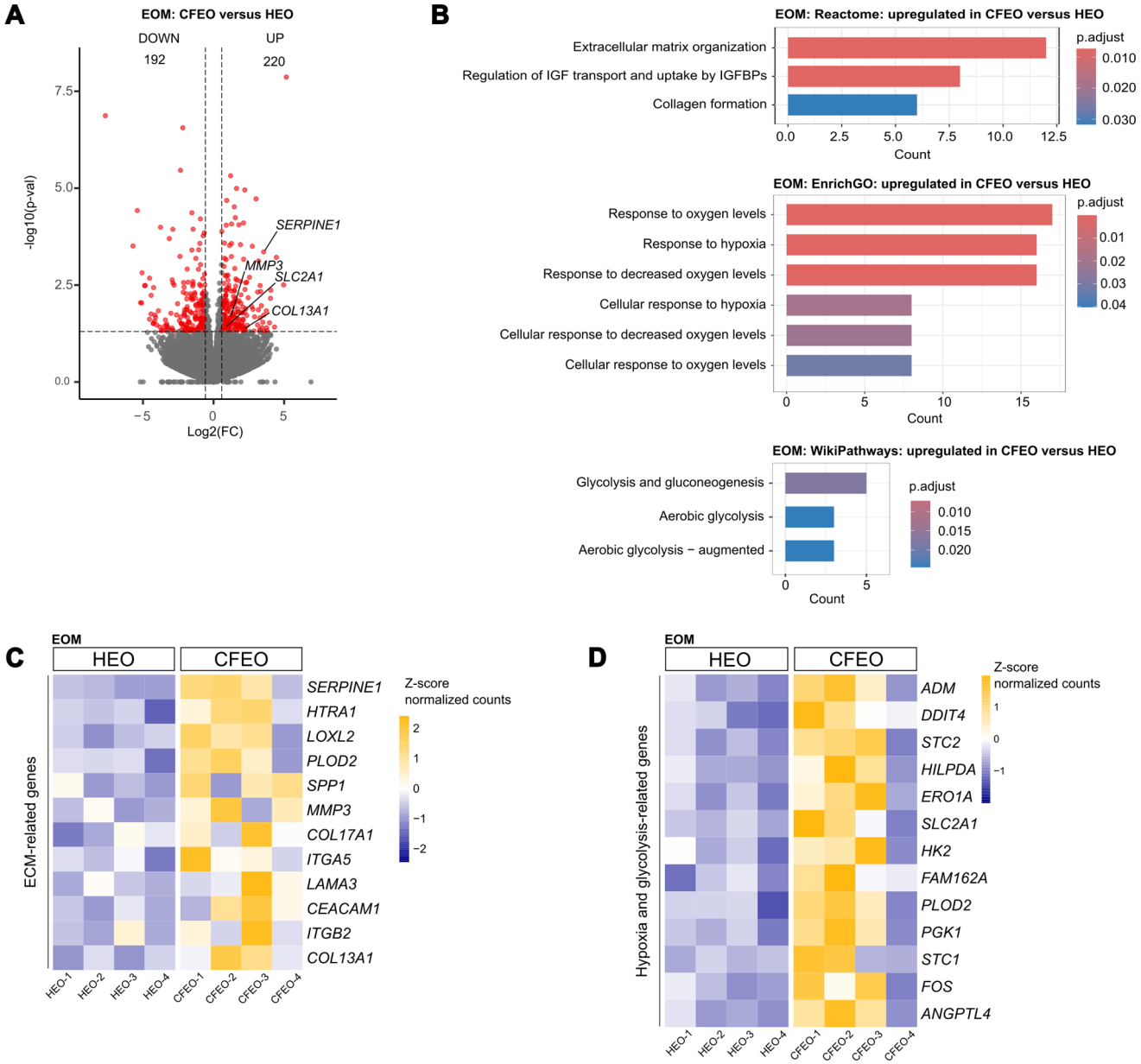

Fig. 3 Transcriptomic analysis of CF and healthy endometrial organoids in basal culture condition. **A** Volcano plot with log2(fold change (FC)) *versus*–log10(p-value) showing up- (right) and down (left)-regulated genes (red) in CFEO *versus* HEO in EOM, as extracted from bulk RNA-seq data. Number of DEGs is shown, and genes mentioned in the text are indicated. **B** GO analysis of genes upregulated in CFEO *versus* HEO in EOM. **C**, **D** Heatmap displaying scaled expression (represented as z-score of normalized counts, see color scale) of indicated ECM- (**C**) and hypoxia- and glycolysis- (**D**) related genes in HEO and CFEO, as extracted from bulk RNA-seq data

cells. Using unsupervised clustering, UMAP visualization and canonical cell type-specific gene signatures [23–25], 17 distinct clusters were identified including endometrial (proliferating (prolif)) epithelial and (superficial and deep) stromal cells (SC), pericytes, smooth muscle cells (SMC), endothelial cells (both blood vascular and lymphatic endothelial cells (LEC)), mesothelial cells and immune cells including lymphoid (T cells (T), natural killer cells (NK)) and myeloid cells (macrophages, mast cells, neutrophils and conventional dendritic cells (cDCs)) (Fig. S4C, D), all present in the whole-tissue uterine samples which encompass endometrium, myometrium and perimetrium.

For further downstream analyses focusing on the 'fertility' estrus phase, we omitted the CF diestrus dataset, resulting in 26,165 good-quality cells (Fig. 5A, Fig. S4E). Overall, WT and CF uterus-derived cells showed a high degree of overlap, with some apparent separation within the superficial stromal cell cluster (Fig. 5B). *Cftr* expression was most prominently observed in the endometrium epithelial cell population (Fig. 5C), consistent with previous

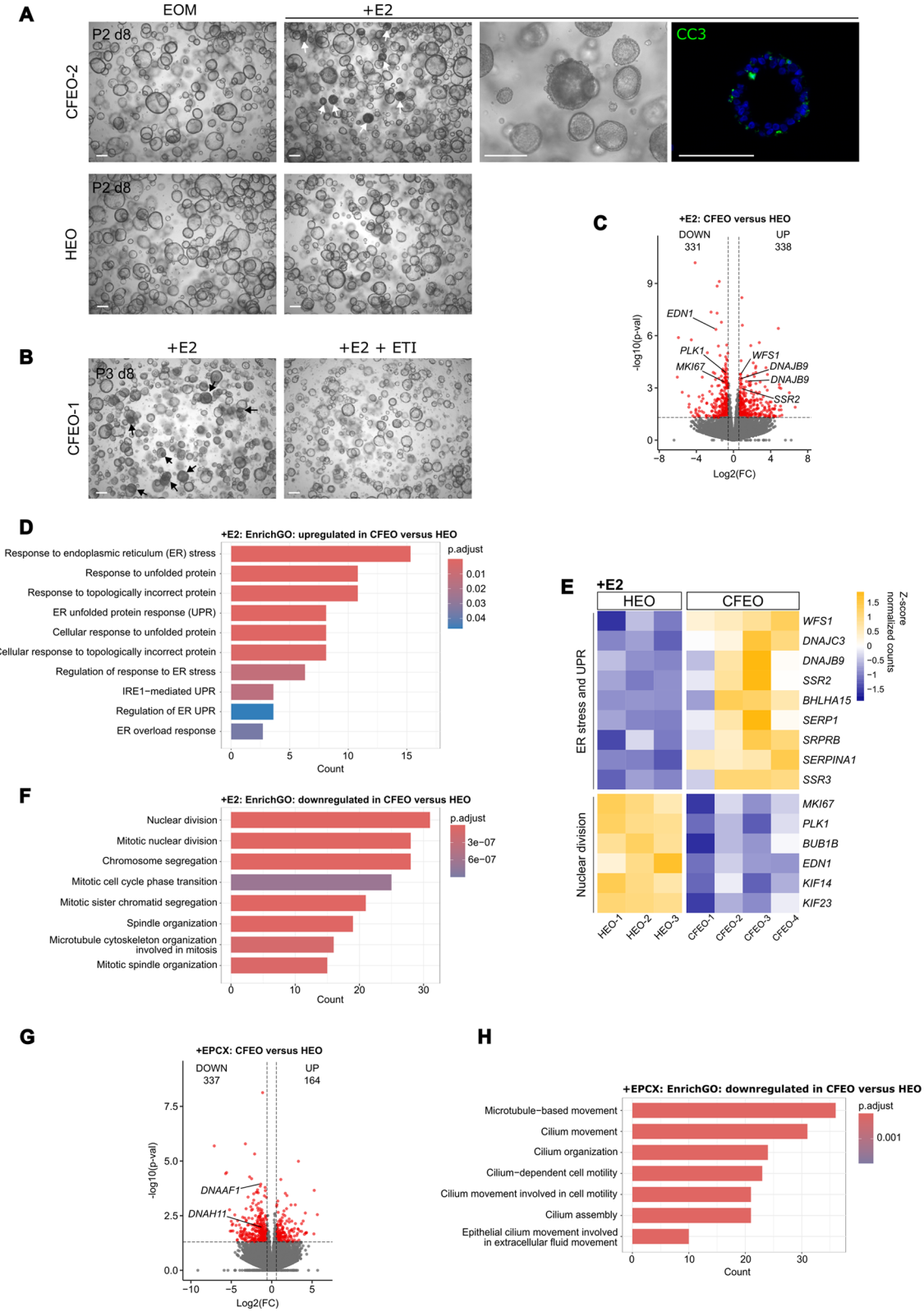
A
EOM
+E2
P2 d8
CFEO-2
CC3
P2 d8
HEO
B
+E2
+E2 + ETI
P3 d8
CFEO-1
C
+E2: CFEO versus HEO
DOWN
331
UP
338
-log10(p-val)
EDN1
PLK1
MKI67
WFS1
DNAJB9
DNAJB9
SSR2
Log2(FC)
D
+E2: EnrichGO: upregulated in CFEO versus HEO
Response to endoplasmic reticulum (ER) stress
Response to unfolded protein
Response to topologically incorrect protein
ER unfolded protein response (UPR)
Cellular response to unfolded protein
Cellular response to topologically incorrect protein
Regulation of response to ER stress
IRE1−mediated UPR
Regulation of ER UPR
ER overload response
p.adjust
0.01
0.02
0.03
0.04
Count
E
+E2
HEO
CFEO
ER stress and UPR
Nuclear division
WFS1
DNAJC3
DNAJB9
SSR2
BHLHA15
SERP1
SRPRB
SERPINA1
SSR3
MKI67
PLK1
BUB1B
EDN1
KIF14
KIF23
HEO-1
HEO-2
HEO-3
CFEO-1
CFEO-2
CFEO-3
CFEO-4
Z-score
normalized counts
F
+E2: EnrichGO: downregulated in CFEO versus HEO
Nuclear division
Mitotic nuclear division
Chromosome segregation
Mitotic cell cycle phase transition
Mitotic sister chromatid segregation
Spindle organization
Microtubule cytoskeleton organization involved in mitosis
Mitotic spindle organization
p.adjust
3e−07
6e−07
Count
G
+EPCX: CFEO versus HEO
DOWN
337
UP
164
-log10(p-val)
DNAAF1
DNAH11
Log2(FC)
H
+EPCX: EnrichGO: downregulated in CFEO versus HEO
Microtubule−based movement
Cilium movement
Cilium organization
Cilium−dependent cell motility
Cilium movement involved in cell motility
Cilium assembly
Epithelial cilium movement involved in extracellular fluid movement
p.adjust
0.001
Count

Fig. 4 Phenotypic and transcriptomic responses of CFEO to hormone exposure. **A** HEO and CFEO cultures (P2, d8) in EOM (without hormones) and upon E2 exposure. Arrows indicate dark organoids (magnified in third panel). Immunofluorescence staining of CC3 (right panel). Representative BF images are shown. **B** CFEO culture exposed to E2 supplemented with vehicle (DMSO) or ETI. Arrows indicate dark organoids. Representative BF images are shown. **C** Volcano plot with log2(fold change (FC)) *versus*–log10(p-value) showing up- (right) and down (left)-regulated genes (red) in CFEO *versus* HEO, both exposed to E2, as extracted from bulk RNA-seq data. Number of DEGs is shown, and genes mentioned in the text are indicated. **D** GO analysis of genes upregulated in CFEO *versus* HEO, both exposed to E2. **E** Heatmap displaying scaled expression (represented as z-score of normalized counts, see color scale) of indicated ER stress/UPR- and nuclear division-related genes in HEO and CFEO (both exposed to E2), as extracted from bulk RNA-seq data. **F** GO analysis of genes downregulated in CFEO *versus* HEO, both exposed to E2. **G** Volcano plot with log2(fold change (FC)) *versus*–log10(p-value) showing up- (right) and down (left)-regulated genes (red) in CFEO *versus* HEO, both exposed to EPCX, as extracted from bulk RNA-seq data. Number of DEGs is shown, and genes mentioned in the text are indicated. **H** GO analysis of genes downregulated in CFEO *versus* HEO, both exposed to EPCX

reports [5]. Therefore, we focused our further analyses on this cell cluster. Epithelial cells were less abundant in CF than WT (Fig. 5B, D), in line with the reduced presence of epithelial glands in CF *versus* WT uterus as observed through H&E staining (Fig. S4F). Bioinformatic analysis of the epithelial cell cluster (excluding the small proliferating cluster) revealed 2,050 significant DEGs (FDR < 0.05 and avg_log2FC > 0.50) between CF and WT (Table S5A). Interestingly, GO analysis of upregulated DEGs in CF epithelial cells (Table 5SB, C) revealed enrichment of biological terms/processes similar to the ones enriched in human CFEO *versus* HEO (Fig. 3B), i.e. ECM-related (cell–ECM interactions, integrin signaling), hypoxia and IGF pathways (Fig. 5E). In addition, upregulated cellular stress, apoptosis terms and estrogen/ESR signaling (Fig. 5E) may also correlate with findings in human CFEO (see above). Furthermore, WNT and immune/inflammation/cytokine signaling pathways were found enriched in CF compared to WT endometrial epithelium (Fig. S4G), all identified to be important in CF [55–57]. In accordance with the upregulated immune-associated pathways, immune cells are more abundant in the CF uterus (Fig. 5D). Interestingly, in the scRNA-seq data the neutrophil cluster is almost exclusively derived from CF (but not WT) uteri (Fig. 5B), concordant with neutrophil inflammatory influx as typical hallmark of CF (as, for instance, detected in the airways) [57]. We observed the presence of particular cells under the luminal epithelium in the CF (but not WT) endometrium, likely representing phagocytic neutrophils (Fig. S4F).

Together, our findings show specific changes in the CF mouse endometrium which are comparable to those found in CF human endometrial organoids and which were previously associated with CF in other tissues.

Organoids can be developed from CF mouse endometrium and recapitulate CFTR dysfunction

To enable future exploration of mouse endometrial pathobiology in CF and functional investigation of transcriptome-extracted findings, we also developed organoid models from mouse CF endometrium as done for humans above (Fig. S1A).

By applying our previously established mouse endometrial organoid protocol [8, 12] (see Materials and Methods and Table S1C), we successfully generated endometrial organoids from CF mouse (termed CF mEO) with 100% efficiency, capable of long-term expansion (Fig. 6A), all aspects comparable to organoid development from WT endometrium (as shown before [8] and validated here, Fig. 6A). The organoids express the epithelial markers ECAD and CK8/18 as well as the endometrial (glandular) epithelium marker FOXA2, both in CF and WT conditions (Fig. 6B, and shown before [8]), thereby recapitulating the endometrial epithelium.

Before, we have shown that organoids from healthy mouse endometrium exhibit physiological hormone responsiveness [8]. *Cftr* and *Enac* expression in mouse endometrium are also known to fluctuate in a mirrored fashion during the estrous cycle [5], following a pattern similar to that observed during the menstrual cycle in humans (i.e. higher *Cftr* and lower *Enac* expression in the E2-dominant phase). We confirmed this pattern and found higher *Cftr* expression in the ex vivo endometrium in estrus compared to diestrus and the opposite pattern for *Enac* (which appears most prominent for the a subunit (*Scnn1a*)) (Fig. S5). This expression pattern was found to be recapitulated in the mEO model, showing higher *Cftr* and lower *Enac* expression following E2 exposure (Fig. 6C). Taken together, the findings support that (WT) mEO show the appropriate physiology for CF endometrium research.

As observed for human EO, CF mEO morphology is not different from WT mEO (Fig. 6A). Also here, other ion and fluid-regulating channels such as *Ano1*, *Slc26a9* and *Slc26a4* are expressed in the organoids (with no difference between WT and CF; Fig. 6D), which may explain the inflated phenotype of the CF mEO being comparable to the WT mEO. Also here, we applied the FIS assay to validate CFTR ion channel deficiency. In contrast to the human EO (HEO; Fig. 2D), the WT mEO showed considerable swelling capacity despite their pre-swollen nature (Fig. 6E). CF mEO showed significantly less swelling than WT mEO (Fig. 6E), which could be rescued by exposure to ET (Fig. 6F), both modulators known to rescue mouse *F508del Cftr* [58]. Together, these findings underscore CFTR channel function deficiency in CF mEO. Intriguingly, although FSK-triggered swelling was significantly less than in WT

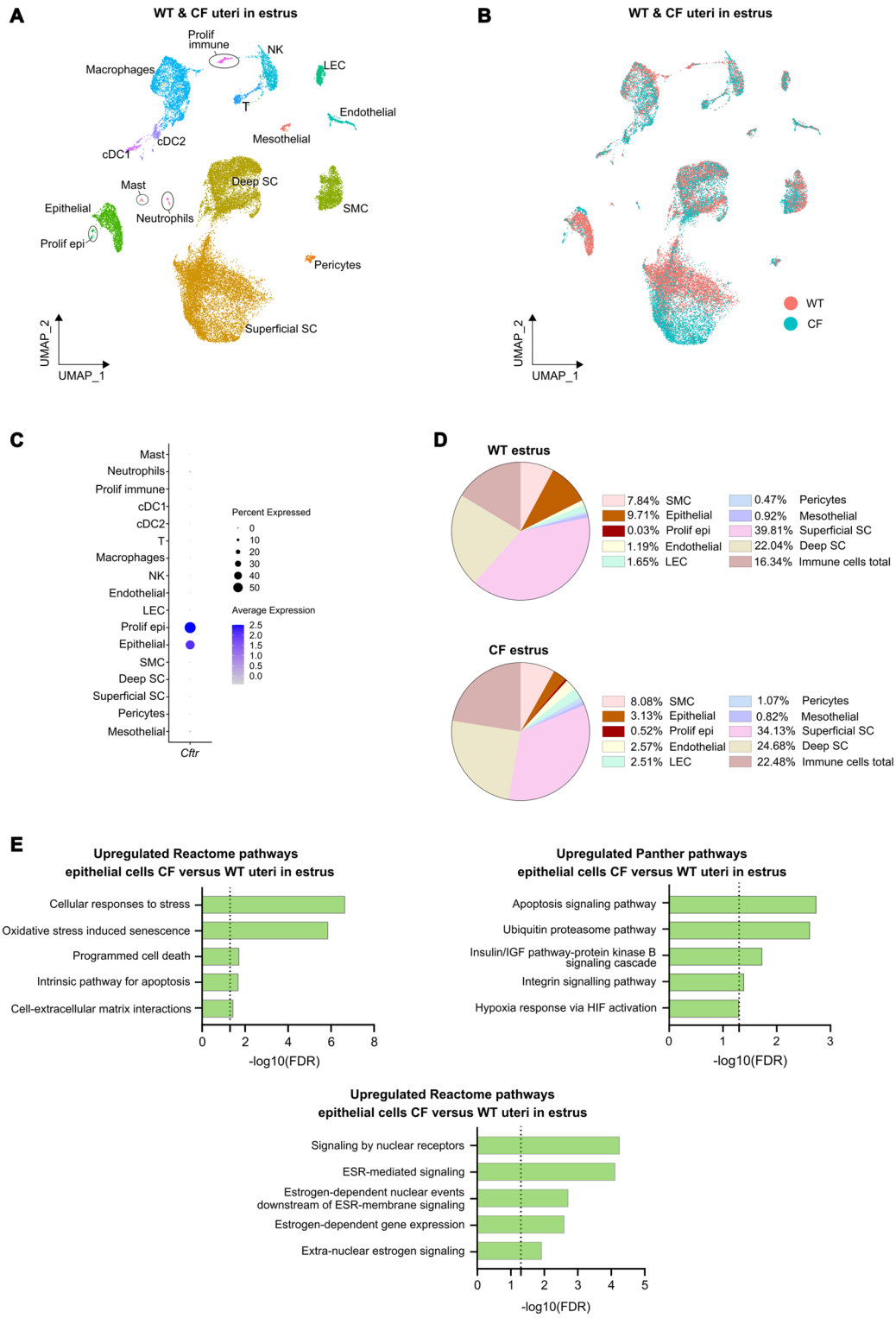

Fig. 5 Single-cell transcriptomics of CF and WT mouse uterus. **A** UMAP plot of the annotated cell clusters in the integrated WT and CF uteri samples in estrus cycle phase. NK, natural killer cells; SC, stromal cells; SMC, smooth muscle cells; Prolif, proliferating; Epi, epithelial cells; cDC, conventional dendritic cells; LEC, lymphatic endothelial cells; T, T cells. **B** UMAP plot visualizing WT and CF uterine cell distribution. **C** Dotplot displaying average expression (color intensity, see scale) of *Cftr* and percentage of expressing cells (dot size, see scale) within the cell clusters. **D** Pie chart showing proportions (%) of each cell cluster in WT (top) and CF (bottom) uteri samples in estrus. **E** Upregulated DEG-associated GO biological processes and terms in CF epithelial cells compared to WT epithelial cells from uteri in estrus

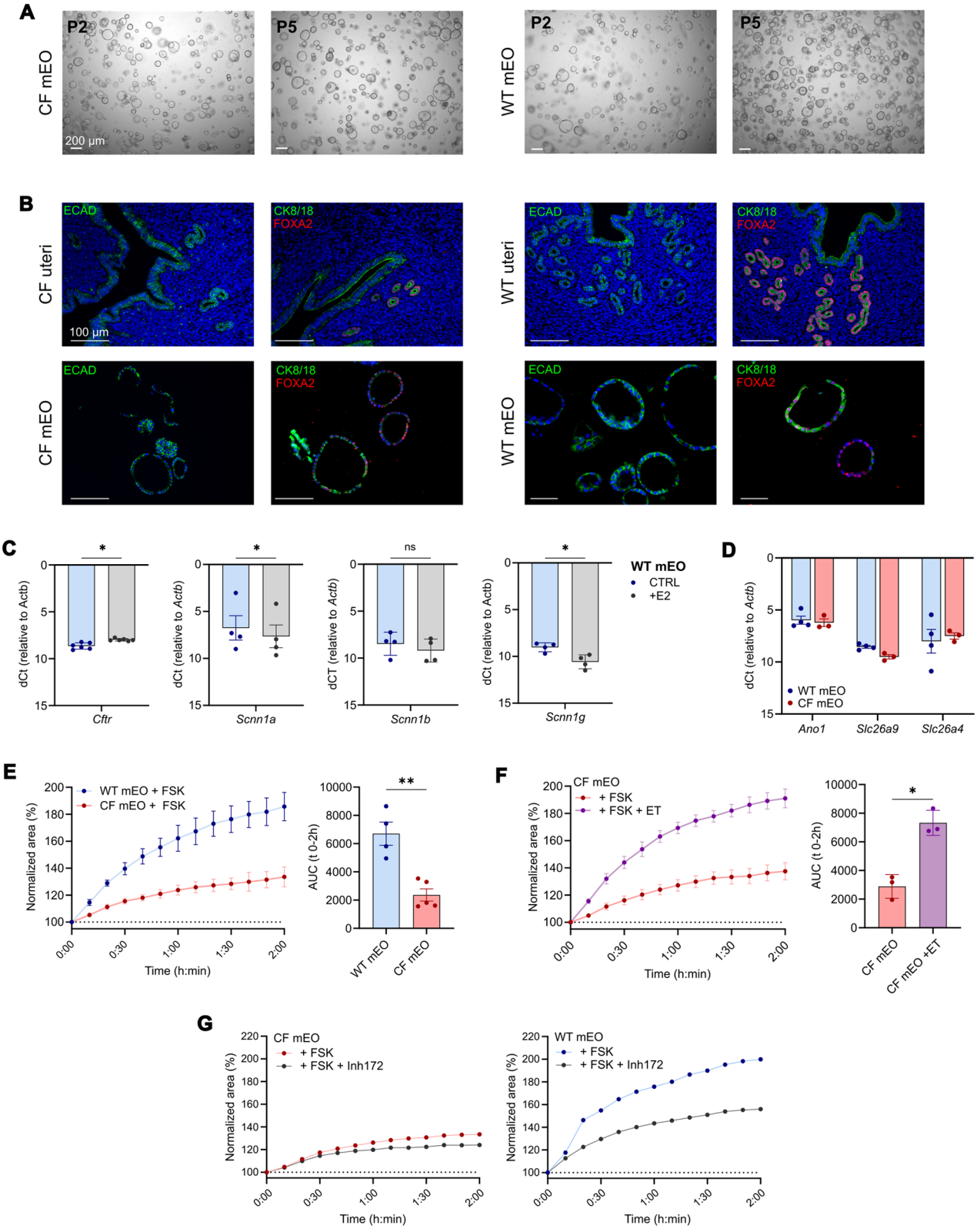
A
CF mEO
P2
P5
200 µm
WT mEO
P2
P5
B
CF uteri
ECAD
CK8/18
FOXA2
100 µm
WT uteri
CF mEO
WT mEO
C
dCt (relative to Actb)
Cftr
Scnn1a
Scnn1b
Scnn1g
WT mEO
CTRL
+E2
D
dCt (relative to Actb)
Ano1
Slc26a9
Slc26a4
WT mEO
CF mEO
E
Normalized area (%)
WT mEO + FSK
CF mEO + FSK
Time (h:min)
AUC (t 0-2h)
WT mEO
CF mEO
F
CF mEO
+ FSK
+ FSK + ET
Normalized area (%)
Time (h:min)
AUC (t 0-2h)
CF mEO
CF mEO +ET
G
CF mEO
+ FSK
+ FSK + Inh172
Normalized area (%)
Time (h:min)
WT mEO
+ FSK
+ FSK + Inh172
Normalized area (%)
Time (h:min)

Fig. 6 Establishment and characterization of mouse CF endometrial organoids. **A** Organoid culture in P2 (left) and P5 (right) from WT (WT mEO) and CF (CF mEO) mouse endometrium. Representative BF images are shown. **B** Immunofluorescence staining for ECAD, CK8/18 and FOXA2 in CF (left) and WT (right) mouse uterine tissue (top) and mEO (bottom). **C** Bar graphs showing relative gene expression levels of indicated genes in WT mEO with and without (control, CTRL) exposure to E2, as determined by RT-qPCR. Data are mean ± SEM of $n=6$ (*Cftr*) or $n=4$ (*Scnn1a*, *b*,*g*) biological replicates (indicated by data points); two-tailed paired t-test; $*p<0.05$, ns: not significant. **D** Bar graphs showing relative gene expression levels of indicated genes in WT mEO and CF mEO as determined by RT-qPCR. Data are mean ± SEM of $n=4$ (WT mEO) and $n=3$ (CF mEO) biological replicates (indicated by data points). **E** FSK-induced swelling (FIS) in WT and CF mEO ($n=4$ biological replicates for WT mEO, $n=5$ for CF mEO); two-tailed unpaired t-test; $**p<0.01$. **F** Comparison of FIS in CF mEO, treated with vehicle (DMSO) or ET ($n=3$ biological replicates); two-tailed paired t-test; $*p<0.05$. **G** FIS in WT mEO (left, $n=1$ biological replicate) and CF mEO (right, $n=2$ biological replicates with mean shown), treated with vehicle (DMSO) or Inh172. **E**, **F**, **G** Graphs (left) indicate FIS quantification as percentage change in surface area relative to t = 0 (normalized area). Bar graphs (right) show area under the curve (AUC) from t = 0 to 2 h. Data are mean ± SEM of mentioned biological replicates (with indication of data points in bar graphs)

mEO, the CF mEO still showed some residual swelling (Fig. 6E, F). Inh172 pre-treatment of CF mEO did not considerably reduce the swelling, whereas it did in WT mEO, although also not completely (Fig. 6G), suggesting that the remaining swelling after Inh172 treatment in both CF and WT mEO may be explained by the presence and activation of other ion/fluid channels present, as reported also for other CF organoid models [37–39].

Taken together, we succeeded in developing long-term expandable endometrial organoids from CF mouse. The organoids exhibit CFTR dysfunction and respond to CFTR modulator treatment, which validates also this model to investigate the impact of CFTR (dys)function, as well as CFTR modulators, in endometrium (patho)biology.

Discussion

The increase in quality and life expectancy of CF patients because of HEMT has put CF co-morbidities, such as fertility problems, more at the forefront. The contribution of dysfunctional endometrial CFTR and resultant endometrial pathobiology to decreased female fertility is unknown, mainly due to the lack of relevant study models. Here, we applied organoid technology, known to reliably capture tissue (patho)biology in vitro, to develop the first endometrial organoid models from human and mouse CF endometrium.

CFTR dysfunction in CFEO was confirmed using FIS and HS-YFP assays, in particular also showing (partial) rescue by CFTR modulators, being the first demonstration of direct HEMT impact on endometrial tissue, (as revealed here by its organoids). Pregnancies in wwCF have increased in the HEMT era [59], but this improvement has so far not been associated with impacts at the level of the endometrium, which should now be considered based on our findings. In addition, the organoid model provides the opportunity to test the effects of current and future CFTR modulators on endometrial (dys)function in wwCF, even in a personalized medicine approach.

The CFEO recapitulated key aspects of CF. Pathway differences in CFEO compared to HEO included upregulated ECM (re-)modeling and hypoxia, both found in other CF-affected tissues. For instance, tissue remodeling with enhanced collagen formation and deposition has been described in CF lung and liver [41, 42], as well as in vitro CF models [43]. Interestingly, we found increased expression of plasminogen activator inhibitor-1 (PAI-1 or SERPINE-1) in CFEO. Plasminogen and its active form, plasmin, play crucial roles in ECM remodeling, wound healing and tissue repair by degrading ECM components [60]. Enhanced inhibition of these processes (by PAI-1) in CF could lead to dysfunctional wound healing and tissue repair, processes essential during physiological menstrual cycling. Hypoxia can further contribute to these processes since PAI-1 is a target gene of hypoxia-inducible factor-1 (HIF-1) [61]. CF patients (and derived tissue cells) exhibit increased O_2 and energy consumption, as shown in CF nasal polyp epithelium [45, 62]. Enhanced O_2 consumption may lead to hypoxia which in turn changes cellular metabolism toward glycolysis [46], also in line with our finding of enriched glycolysis in CFEO. The increased hypoxia phenotype in CFEO, observed in the absence of hypoxic culture conditions, suggests that this hypoxic signature is a direct effect of CFTR dysfunction, as also reported in endothelial cells upon CFTR-silencing [44].

Interestingly, our study uncovered aberrant hormonal responses in CFEO. Exposure to E2, mimicking the proliferative phase of the menstrual cycle, revealed several enriched pathways, in particular enhanced ER stress/UPR and cell cycle arrest. ER stress and UPR may in the first place be linked to retained misfolded *F508del* CFTR protein in the ER [63, 64]. However, these pathways were only found significantly enriched when E2 was added to the CFEO. E2 signaling indeed leads to enhanced overall protein production [65] and can induce ER stress, via estrogen receptor signaling, as found in other (diseased) tissues [66, 67]. We hypothesize that E2 exposure together with UPR, triggered by misfolded *F508del* CFTR, raises the ER stress level above a certain threshold that eventually triggers cell cycle arrest. Apparently, some cells even enter into apoptosis as observed in E2-exposed CFEO, but not HEO, cultures. Indeed, when UPR fails to constrain ER stress, ER stress ultimately results in apoptosis [50]. Interestingly, CFTR

modulator treatment could prevent the apoptotic events in E2-exposed CFEO, suggesting that by reducing ER stress and UPR burden, proteostasis control can be regained. Thus, the observed increased fertility in wwCF upon HEMT [68] may (also) be linked to the restoration of defective CFTR in the endometrium. Further research into the underlying pathways of the aberrant hormone responses will be important, in particular since 15% of wwCF are not eligible for HEMT [35]. Therapeutic targets within pathways, including the ones identified here, may pose alternative options to increase reproductive fitness and chances of pregnancy in wwCF. Exposure to EPCX, mimicking the (mid-)secretory (receptive) phase of the menstrual cycle, revealed decreased cilia-related pathways (organization/assembly/movement) in CFEO *versus* HEO. Ciliated endometrial cells coordinate fluid and particle movement across the surface of the endometrium, which is essential for proper positioning and orientation of the embryo within the uterine cavity during implantation. Cilia are thus key players in the endometrium's receptivity for the embryo, and defective assembly or function may thus contribute to the decreased fertility in wwCF. Primary cilia dyskinesia, another genetic disease in which cilium motility is negatively impacted (some of which due to genetic mutation in *DNAH11*, the gene we found downregulated in CFEO) has indeed been associated with female infertility [69]. Recently, we established a human in vitro implantation model, in which interactions between embryo and endometrium are faithfully reproduced [10]. The establishment and biobanking of CFEO, as done here, enable to employ CF endometrium in this implantation model to investigate the effect of aberrant processes (e.g. downregulated cilia assembly and activity) on embryo implantation.

While patient-derived organoids are highly valuable, certainly for the clinical situation and prospective personalized medicine studies [70–73], a mouse model allows for direct in vivo interference with identified dysregulated pathways through antibodies, small molecules or genetic modifications (such as knockdown or knock-out). Additionally, mice provide a preclinical platform for drug development, enabling the testing of therapeutic interventions targeting identified pathways. Therefore, we expanded the experimental toolbox to explore CF endometrial pathobiology by implementing the CF *F508del* mouse model. Single-cell transcriptomics revealed in the CF endometrial epithelium enriched cell–ECM interactions and integrin signaling, hypoxia, IGF pathway and apoptosis compared to WT epithelium, findings similar to the ones in the human (epithelial) CFEO, thereby reinforcing our observations in human CF endometrium as well as validating the translatability of the CF mouse model to the human setting which will be highly useful in future studies. Together, the combination of human and mouse endometrial organoid models will offer reinforcing and complementary insights into CF endometrial pathobiology.

An additional enriched pathway found in mouse CF endometrial epithelium is WNT. It has previously been reported that the CFTR interactome encompasses β-catenin [74, 75], the central mediator of the canonical WNT pathway, and that CF-linked defective CFTR is associated with aberrantly elevated WNT/β-catenin signaling (as found in intestinal crypt and kidney epithelium [55, 56]).

This first scRNA-seq profiling of CF mouse uterus (in comparison to WT uterus) provides a highly valuable resource to deeply investigate CF implications in the uterus as a whole at both a molecular, pathway and cellular level and will enable target selection for translation into human clinical studies and applications. For instance, the mouse CF uterus presented with lower abundance of epithelial cells and higher number of immune cells compared to WT. In addition, we observed a separation in the (superficial) stromal cell cluster between WT and CF uterus. Although CFTR expression (thus activity) is mainly located in epithelial cells, abnormalities in stromal cells have been shown before in the CF airway [76]. In the endometrium, crosstalk between epithelial and stromal cells is crucial for proper functioning toward pregnancy [77, 78]. Hence, it will be interesting to deeply explore epithelial-stromal interactions and crosstalk in CF *versus* WT endometrium, as enabled by our scRNA-seq atlas.

In conclusion, our newly developed patient and mouse endometrial organoid models present a valuable platform for studying CF-associated endometrial pathobiology, addressing a significant gap in understanding fertility deficiency faced by wwCF. The aberrations identified in CF endometrium such as dysregulated ECM remodeling, altered hormonal responses and increased apoptosis, can lead to impaired endometrial receptivity and suboptimal conditions for implantation and pregnancy, thus collectively contributing to the decreased fertility in wwCF. Understanding underlying mechanisms is crucial, particularly as advancements in CF therapies have led to increased life expectancy, allowing more CF patients to consider starting families. Our results and models will enable to explore new avenues for addressing the fertility challenges in wwCF.

Supplementary Information The online version contains supplementary material available at https://doi.org/10.1007/s00018-025-05627-7.

Acknowledgements We thank our other colleagues (H. Vankelecom group) for their valuable input and technical help, especially Berkehür Abaylı for the help using the THUNDER Imager. We acknowledge the Leuven Viral Vector Core for HS-YFP vector production, VIB Nucleomics Core for bulk RNA-seq library preparation and sequencing, and the Genomics Core (especially Álvaro Cortés Calabuig) for

statistical data analysis of bulk RNA-seq data and raw scRNA-seq data processing. We thank Teresinha Leal for kindly gifting us the *Cftr*^{tm1Eur} mouse model. We would also like to thank the CF patients and hospital staff who participated in this study, especially Nele Duplacie for the help in CF patient recruitment and informed consent procedure.

Author contributions E. De Pauw, B. Gommers, M.S. Carlon and H. Vankelecom conceptualized the research questions and co-interpreted the results; E. De Pauw, B. Gommers, M.M. Ensinck performed all experiments, data analyses, and interpreted the results; S. Timmerman collected CF endometrial biopsies; S. De Vriendt and C. Bueds processed (raw) scRNA-seq data and assisted in bioinformatical analyses; M. Wei and C. Bueds assisted in bioinformatical analyses of bulk RNA-seq data; F. Hermans assisted in bioinformatical analyses and co-discussed certain results; K. Arnauts and A.S. Ramalho provided organoid medium components and know-how; A.S. Ramalho and F. Vermeulen provided CF rectal organoid pictures; L. Dupont supervised patient recruitment; D. Lambrechts co-supervised the scRNA-seq experiments; E. De Pauw prepared the figures; E. De Pauw and H. Vankelecom supervised all work and wrote the manuscript.
All co-authors critically read and approved the manuscript.

Funding This work was supported by a joint grant from the Fund Alphonse-Jean Forton (King Baudouin Foundation) and Belgian CF patient association (2023-J1810150-232650). E. De Pauw (11E9321N), S. De Vriendt (1S00823N), C. Bueds (1129323 N) are supported by a PhD Fellowship from the Fonds voor Wetenschappelijk Onderzoek (FWO) Vlaanderen. M. Wei is supported by a PhD grant from China Scholarship Council. M.M. Ensinck (1282925 N) and F. Hermans (1226325 N) are supported by a Postdoctoral Fellowship from FWO.

Data availability Bulk RNA-seq and scRNA-seq data have been deposited to the ArrayExpress database (accession numbers E-MTAB-14456 and E-MTAB-14455). All raw and analyzed sequencing data from the publicly available dataset [31] that was used in Fig. S1 can be found at NCBI's Gene Expression Omnibus (series accession code GSE111976). Further data that support the findings discussed here are available from the corresponding author upon reasonable request.

Declarations

Ethical approval The study was approved by the Ethical Research Committee UZ/KU Leuven (endometrial biopsies; S66294, S59006, S65570, rectal biopsies; S56329) and is compliant with all relevant ethical regulations regarding research involving human participants. All animal experiments were approved by the KU Leuven Ethical Committee for Animal Experimentation (P072/2024).

Consent to participate Informed consent was obtained from all individual participants included in the study.

Consent to publish All human participants provided written informed consent for use of their data for publication after study information was given.

Conflict of interest The authors declare no competing financial interests.

References

1. Ahmad A, Ahmed A, Patrizio P (2013) Cystic fibrosis and fertility. Curr Opin Obstet Gynecol 25(3):167–172. https://doi.org/10.1097/GCO.0b013e32835f1745
2. Shteinberg M et al (2019) Failure to conceive in women with CF is associated with pancreatic insufficiency and advancing age. J Cyst Fibros 18:525–529. https://doi.org/10.1016/j.jcf.2018.10.009
3. Wang XF et al (2003) Involvement of CFTR in uterine bicarbonate secretion and the fertilizing capacity of sperm. Nat Cell Biol 5(10):902–906. https://doi.org/10.1038/ncb1047
4. Zheng XY, Chen GA, Wang HY (2004) Expression of cystic fibrosis transmembrane conductance regulator in human endometrium. Hum Reprod 19(12):2933–2941. https://doi.org/10.1093/humrep/deh507
5. Chan LN et al (2002) Distribution and regulation of ENaC subunit and CFTR mRNA expression in murine female reproductive tract. J Membr Biol 185(2):165–176. https://doi.org/10.1007/s00232-001-0117-y
6. Ruan YC, Chen H, Chan HC (2014) Ion channels in the endometrium: regulation of endometrial receptivity and embryo implantation. Hum Reprod Update 20(4):517–529. https://doi.org/10.1093/humupd/dmu006
7. Yang JZ et al (2004) Differential expression and localization of CFTR and ENaC in mouse endometrium during pre-implantation. Cell Biol Int 28(6):433–439. https://doi.org/10.1016/j.cellbi.2004.03.011
8. Boretto M et al (2017) Development of organoids from mouse and human endometrium showing endometrial epithelium physiology and long-term expandability. Development 144(10):1775–1786. https://doi.org/10.1242/dev.148478
9. Boretto M et al (2019) Patient-derived organoids from endometrial disease capture clinical heterogeneity and are amenable to drug screening. Nat Cell Biol 21(8):1041–1051. https://doi.org/10.1038/s41556-019-0360-z
10. Kagawa H et al (2022) Human blastoids model blastocyst development and implantation. Nature 601(7894):600–605. https://doi.org/10.1038/s41586-021-04267-8
11. Van Doorninck JH et al (1995) A mouse model for the cystic fibrosis ΔF508 mutation. EMBO J 14(18):4403–4411. https://doi.org/10.1002/j.1460-2075.1995.tb00119.x
12. Tang S, Parks SE, Liao Z, Cope DI, Blutt SE, Monsivais D (2023) Establishing 3D endometrial organoids from the mouse uterus. J Visualized Experiments 6:(191). https://doi.org/10.3791/64448
13. Vonk AM et al (2020) Protocol for application, standardization and validation of the forskolin-induced swelling assay in cystic fibrosis human colon organoids. STAR Protoc 1(1):100019. https://doi.org/10.1016/j.xpro.2020.100019
14. Ensinck MM et al (2022) Novel CFTR modulator combinations maximise rescue of G85E and N1303K in rectal organoids. ERJ Open Res 8(2):00716–2021. https://doi.org/10.1183/23120541.00716-2021

15. Ensinck MM et al (2020) Phenotyping of rare CFTR mutations reveals distinct trafficking and functional defects. Cells 9(3):1–14. https://doi.org/10.3390/cells9030754
16. Andrews S (2010) FastQC: a quality control tool for high throughput sequence data. http://www.bioinformatics.babraham.ac.uk/projects/fastqc
17. Bolger AM, Lohse M, Usadel B (2014) Trimmomatic: A flexible trimmer for illumina sequence data. Bioinformatics 30(15):2114–2120. https://doi.org/10.1093/bioinformatics/btu170
18. Kim D, Paggi JM, Park C, Bennett C, Salzberg SL (2019) Graph-based genome alignment and genotyping with HISAT2 and HISAT-genotype. Nat Biotechnol 37(8):907–915. https://doi.org/10.1038/s41587-019-0201-4
19. Liao Y, Smyth GK, Shi W (2016) The Subread aligner: fast, accurate and scalable read mapping by seed-and-vote. Nucleic Acids Res 41(10):e108. https://doi.org/10.1093/nar/gkt214
20. Love MI, Huber W, Anders S (2014) Moderated Estimation of fold change and dispersion for RNA-seq data with DESeq2. Genome Biol 15(12):550. https://doi.org/10.1186/s13059-014-0550-8
21. Hao Y et al (2024) Dictionary learning for integrative, multimodal and scalable single-cell analysis. Nat Biotechnol 42(2):293–304. https://doi.org/10.1038/s41587-023-01767-y
22. McInnes L, Healy J, Melville J (2020) UMAP: Uniform Manifold Approximation and Projection for Dimension Reduction. http://arxiv.org/abs/1802.03426
23. He JP, Tian Q, Zhu QY, Liu JL (2022) Single-cell analysis of mouse uterus at the invasion phase of embryo implantation. Cell Biosci 12(1):1–14. https://doi.org/10.1186/s13578-022-00749-y
24. Zhang L, Long W, Xu W, Chen X, Zhao X, Wu B (2022) Digital cell atlas of mouse uterus: from regenerative stage to maturational stage. Front Genet 13:847646. https://doi.org/10.3389/fgene.2022.847646
25. Padilla-Banks E et al (2023) Developmental Estrogen exposure in mice disrupts uterine epithelial cell differentiation and causes adenocarcinoma via Wnt/βcatenin and PI3K/AKT signaling. PLoS Biol 21(10):1–32. https://doi.org/10.1371/journal.pbio.3002334
26. McDavid A, Finak G, Yajima M (2023) MAST: Model-based analysis of single cell transcriptomics. https://doi.org/10.18129/B9.bioc.MAST
27. Thomas PD, Ebert D, Muruganujan A, Mushayahama T, Albou LP, Mi H (2022) PANTHER: making genome-scale phylogenetics accessible to all. Protein Sci 31(1):8–22. https://doi.org/10.1002/pro.4218
28. Laporte E et al (2022) Decoding the activated stem cell phenotype of the neonatally maturing pituitary. Elife 11:e75742. https://doi.org/10.7554/eLife.75742
29. Seishima R et al (2019) Neonatal Wnt-dependent Lgr5 positive stem cells are essential for uterine gland development. Nat Commun 10(1):5378. https://doi.org/10.1038/s41467-019-13363-3
30. Garcia-Alonso L et al (2021) Mapping the Temporal and Spatial dynamics of the human endometrium in vivo and in vitro. Nat Genet 53(12):1698–1711. https://doi.org/10.1038/s41588-021-00972-2
31. Wang W et al (2020) Single-cell transcriptomic atlas of the human endometrium during the menstrual cycle. Nat Med 26(10):1644–1653. https://doi.org/10.1038/s41591-020-1040-z
32. Zomer-van Ommen DD et al (2018) Comparison of ex vivo and in vitro intestinal cystic fibrosis models to measure CFTR-dependent ion channel activity. J Cyst Fibros 17(3):316–324. https://doi.org/10.1016/j.jcf.2018.02.007
33. Gholami K, Muniandy S, Salleh N (2013) In-vivo functional study on the involvement of CFTR, SLC26A6, NHE-1 and CA isoenzymes II and XII in uterine fluid pH, volume and electrolyte regulation in rats under different sex-steroid influence. Int J Med Sci 10(9):1121–1134. https://doi.org/10.7150/ijms.5918
34. Xie ZD et al (2018) The balance of HCO3-Secretion vs. reabsorption in the endometrial epithelium regulates uterine fluid pH. Front Physiol 9:12. https://doi.org/10.3389/fphys.2018.00012
35. Ensinck MM, Carlon MS (2022) One size does not fit all: the past, present and future of CF causal therapies. Cells 11(12):1–44. https://doi.org/10.3390/cells11121868
36. Dekkers JF et al (2016) Characterizing responses to CFTR-modulating drugs using rectal organoids derived from subjects with cystic fibrosis. Sci Transl Med 8(344):344ra84. https://doi.org/10.1126/scitranslmed.aad8278
37. Amatngalim GD et al (2022) Measuring cystic fibrosis drug responses in organoids derived from 2D differentiated nasal epithelia. Life Sci Alliance 5(12):1–14. https://doi.org/10.26508/lsa.202101320
38. Sachs N et al (2019) Long-term expanding human airway organoids for disease modeling. EMBO J 38(4):e100300. https://doi.org/10.15252/embj.2018100300
39. Rodenburg LW et al (2022) Drug repurposing for cystic fibrosis: identification of drugs that induce CFTR-independent fluid secretion in nasal organoids. Int J Mol Sci 23(20):12657. https://doi.org/10.3390/ijms232012657
40. Thiagarajah JR, Song Y, Haggie PM, Verkman AS (2004) A small molecule CFTR inhibitor produces cystic fibrosis-like submucosal gland fluid secretions in normal airways. FASEB J 18(7):875–877. https://doi.org/10.1096/fj.03-1248fje
41. Lindblad A, Hultcrantz R, Strandvik B (1992) Bile-duct destruction and collagen deposition: A prominent ultrastructural feature of the liver in cystic fibrosis. Hepatology 16(2):372–381. https://doi.org/10.1002/hep.1840160215
42. Harris WT et al (2013) Myofibroblast differentiation and enhanced TGF-B signaling in cystic fibrosis lung disease. PLoS ONE 8(8):e70196. https://doi.org/10.1371/journal.pone.0070196
43. Mazio C et al (2024) A functional 3D full-thickness model for comprehending the interaction between airway epithelium and connective tissue in cystic fibrosis. Biomaterials 308:122546. https://doi.org/10.1016/j.biomaterials.2024.122546
44. Declercq M et al (2021) Transcriptomic analysis of CFTR-impaired endothelial cells reveals a pro-inflammatory phenotype. Eur Respir J 57(4):2000261. https://doi.org/10.1183/13993003.00261-2020
45. Stutts MJ, Knowles MR, Gatzy JT, Boucher RC (1986) Oxygen consumption and Ouabain binding sites in cystic fibrosis nasal epithelium. Pediatr Res 20(12):1316–1320. https://doi.org/10.1203/00006450-198612000-00026
46. Kierans SJ, Taylor CT (2021) Regulation of Glycolysis by the hypoxia-inducible factor (HIF): implications for cellular physiology. J Physiol 599(1):23–37. https://doi.org/10.1113/JP280572
47. Kierans SJ et al (2023) Hypoxia induces a glycolytic complex in intestinal epithelial cells independent of HIF-1-driven glycolytic gene expression. Proc Natl Acad Sci USA 120(35):e2208117120. https://doi.org/10.1073/pnas.2208117120
48. Daisuke K et al (2002) Hypoxia enhances the expression of plasminogen activator inhibitor-1 in human lung cancer cells, EBC-1. Tohoku J Exp Med 196(4):259–267. https://doi.org/10.1620/tjem.196.259
49. Thomas K, Roth U, Jungermann K (1999) Induction of the plasminogen activator inhibitor-1 gene expression by mild hypoxia via a hypoxia response element binding the hypoxia-inducible factor-1 in rat hepatocytes. Blood 94(12):4177–4185
50. Hetz C (2012) The unfolded protein response: controlling cell fate decisions under ER stress and beyond. Nat Rev Mol Cell Biol 13(2):89–102. https://doi.org/10.1038/nrm3270
51. Garg B, Pathria G, Wagner C, Maurer M, Wagner SN (2016) Signal sequence receptor 2 is required for survival of human

melanoma cells as part of an unfolded protein response to Endoplasmic reticulum stress. Mutagenesis 31(5):573–582. https://doi.org/10.1093/mutage/gew023
52. Newman L et al (2023) The impact of primary ciliary dyskinesia on female and male fertility: a narrative review. Hum Reprod Update 29(3):347–367. https://doi.org/10.1093/humupd/dmad003
53. Hodges CA, Palmert MR, Drumm ML (2008) Infertility in females with cystic fibrosis is multifactorial: evidence from mouse models. Endocrinology 149(6):2790–2797. https://doi.org/10.1210/en.2007-1581
54. Shteinberg M, Taylor-Cousar JL, Durieu I, Cohen-Cymberknoh M (2021) Fertility and pregnancy in cystic fibrosis. Chest 160(6):2051–2060. https://doi.org/10.1016/j.chest.2021.07.024
55. Strubberg AM et al (2018) Cftr modulates Wnt/β-Catenin signaling and stem cell proliferation in murine intestine. Cell Mol Gastroenterol Hepatol 5(3):253–271. https://doi.org/10.1016/j.jcmgh.2017.11.013
56. Zhang JT et al (2017) Defective CFTR leads to aberrant β-catenin activation and kidney fibrosis. Sci Rep 7(1):5233. https://doi.org/10.1038/s41598-017-05435-5
57. Roesch EA, Nichols DP, Chmiel JF (2018) Inflammation in cystic fibrosis: an update. Pediatr Pulmonol 53(S3):S30–S50. https://doi.org/10.1002/ppul.24129
58. Bose SJ et al (2019) Differential thermostability and response to cystic fibrosis transmembrane conductance regulator potentiators of human and mouse F508del-CFTR. Am J Physiol Lung Cell Mol Physiol 317(1):L71–L86. https://doi.org/10.1152/ajplung.00034.2019
59. Jain R, Kazmerski TM, Taylor-Cousar JL (2023) The modern landscape of fertility, pregnancy, and parenthood in people with cystic fibrosis. Curr Opin Pulm Med 29(6):595–602. https://doi.org/10.1097/MCP.0000000000001009
60. Castellino FJ, Ploplis VA (2005) Structure and function of the plasminogen/plasmin system. Thromb Haemost 93(4):647–654. https://doi.org/10.1160/TH04-12-0842
61. Krieg AJ, Rankin EB, Chan D, Razorenova O, Fernandez S, Giaccia AJ (2010) Regulation of the histone demethylase JMJD1A by hypoxia-inducible factor 1α enhances hypoxic gene expression and tumor growth. Mol Cell Biol 30(1):344–353. https://doi.org/10.1128/mcb.00444-09
62. Stallings VA et al (2005) Adolescent development and energy expenditure in females with cystic fibrosis. Clin Nutr 24(5):737–745. https://doi.org/10.1016/j.clnu.2005.02.005
63. Bartoszewski R et al (2008) Activation of the unfolded protein response by ΔF508 CFTR. Am J Respir Cell Mol Biol 39(4):448–457. https://doi.org/10.1165/rcmb.2008-0065OC
64. Kerbiriou M, Le Drévo MA, Férec C, Trouvé P (2007) Coupling cystic fibrosis to Endoplasmic reticulum stress: differential role of Grp78 and ATF6. Biochim Biophys Acta Mol Basis Dis 1772(11–12):1236–1249. https://doi.org/10.1016/j.bbadis.2007.10.004
65. Wang Y, Zhu L, Kuokkanen S, Pollard JW (2015) Activation of protein synthesis in mouse uterine epithelial cells by estradiol-17β is mediated by a PKC-ERK 1/2-mTOR signaling pathway. Proc Natl Acad Sci USA 112(11):E1382–E1391. https://doi.org/10.1073/pnas.1418973112
66. Wang C et al (2020) Interaction of estradiol and Endoplasmic reticulum stress in the development of esophageal carcinoma. Front Endocrinol (Lausanne) 11:410. https://doi.org/10.3389/fendo.2020.00410
67. Obiorah IE, Fan P, Sengupta S, Jordan VC (2014) Selective estrogen-induced apoptosis in breast cancer. Steroids 90:60–70. https://doi.org/10.1016/j.steroids.2014.06.003
68. Jones GH, Walshaw MJ (2015) Potential impact on fertility of new systemic therapies for cystic fibrosis. Paediatr Respir Rev 16. https://doi.org/10.1016/j.prrv.2015.07.013. Suppl 1:25–7
69. Schreck LD et al (2024) Infertility and pregnancy outcomes among adults with primary ciliary dyskinesia. Hum Reprod Open 2024(3):hoae039. https://doi.org/10.1093/hropen/hoae039
70. Cuyx S et al (2021) Rectal organoid morphology analysis (ROMA) as a promising diagnostic tool in cystic fibrosis thorax. 76(11):1146–1149. https://doi.org/10.1136/thoraxjnl-2020-216368
71. Muilwijk D et al (2022) Forskolin-induced organoid swelling is associated with long-term cystic fibrosis disease progression. Eur Respir J 60(2):2100508. https://doi.org/10.1183/13993003.00508-2021
72. Ramalho AS et al (2021) Correction of CFTR function in intestinal organoids to guide treatment of cystic fibrosis. Eur Respir J 57(1):1902426. https://doi.org/10.1183/13993003.02426-2019
73. Spelier S et al (2023) High-throughput functional assay in cystic fibrosis patient-derived organoids allows drug repurposing. ERJ Open Res 9(1):00495–2022. https://doi.org/10.1183/23120541.00495-2022
74. Pankow S et al (2015) ΔF508 CFTR interactome remodelling promotes rescue of cystic fibrosis. Nature 528(7583):510–516. https://doi.org/10.1038/nature15729
75. Liu Z et al (2017) CFTR-β-catenin interaction regulates mouse embryonic stem cell differentiation and embryonic development. Cell Death Differ 24(1):98–110. https://doi.org/10.1038/cdd.2016.118
76. Mazio C et al (2020) Intrinsic abnormalities of cystic fibrosis airway connective tissue revealed by an in vitro 3D stromal model. Cells 9(6):1371. https://doi.org/10.3390/cells9061371
77. Zipponi M, Cacciottola L, Dolmans MM (2024) Overview of crosstalk between stromal and epithelial cells in the pathogenesis of adenomyosis and shared features with deep endometriotic nodules. Hum Reprod 39(8):1608–1617. https://doi.org/10.1093/humrep/deae116
78. Yang JH et al (2007) Altered apoptosis and proliferation in endometrial stromal cells of women with adenomyosis. Hum Reprod 22(4):945–952. https://doi.org/10.1093/humrep/del493